Supplementary Information for

Probing Berry phase effect in topological surface states

1. **Fourier components of high-harmonic modulation**

2. **Rule out contributions from surface confined quantum well state**

3. **Tight binding Hamiltonian**

4. **Semiclassical Bloch equations**

1. Fourier components of high-harmonic modulation

Suppose that high-harmonics can originate from both electronic states confined at surface and energy bands immerse in crystal bulk, depends on the symmetry properties of the electronic states[S1,S2]. We extract the modulation components by fitting the oscillation curve of even-order harmonics according to

$$y_{\text{fit}} = c_0 + a_1 \cdot \cos(f_1 x - \Phi) + a_2 \cdot \cos(2 f_1 x - \Psi) ,$$

where $f_1 = T_{2\omega}^{-1}$ is the frequency, $T_{2\omega}$ represents the period of SH field, three parameters c_0, a_1, a_2 denote weights of Fourier components, and Φ, Ψ are modulation phases for periodic modulation of $T_{2\omega}$ and $T_{2\omega}/2$, respectively. The fitting is model-independent, with the free parameters being the relative weights and phases of each component. By performing fitting, we can disentangle the high-harmonics originating from TSSs and bulk bands by extracting relevant Fourier components from the periodic modulation curves.

2. Rule out contributions from surface confined quantum well states

We are also aware the role played by other surface-confined states that coexist with the topological surface states[S3]. When the crystal surface exposes in ambient air, a bulk-originated quantum well states (QWS) is induced by surface band bending in ultrathin space-charge layer[S4]. This occurs as the result of absorption-induced doping and chemical rection[S5]. The two-dimensional electron gas (2DEG) resides in the QWS will further undergo a Rashba-type spin splitting with continuous surface doping[S6]. Having taken into account these factors, we conducted measurements of the high-harmonic modulation following an extended period of exposing the crystal surface to ambient air. In figure S1, we present a comparison between the measured modulation of HH spectra from the $Bi_{1.5}Sb_{0.5}Te_{1.7}Se_{1.3}$ (BSTS) surface immediately after cleavage and after a prolonged exposure of 22 hours, at a temperature of 22.0 °C and humidity of 30 %, respectively. We find that there is no significant change in modulation periodicity of even-order harmonics, except the slightly reduced intensity after long time exposure. This finding strongly indicates that the periodic oscillation of $T_{2\omega}$ is primarily influenced by the dynamical evolution of TSSs.

As a comparison, harmonic spectra modulation from $(Bi_{0.8}In_{0.2})_2Se_3$ (BIS) sample has also been measured, as shown in Fig. S2. The slight shifts in the optimal oscillation phase with respect to harmonic orders can be attributed to the quantum well states induced by surface doping. However, the phase shift is still much smaller in compare with the observations from BSTS.

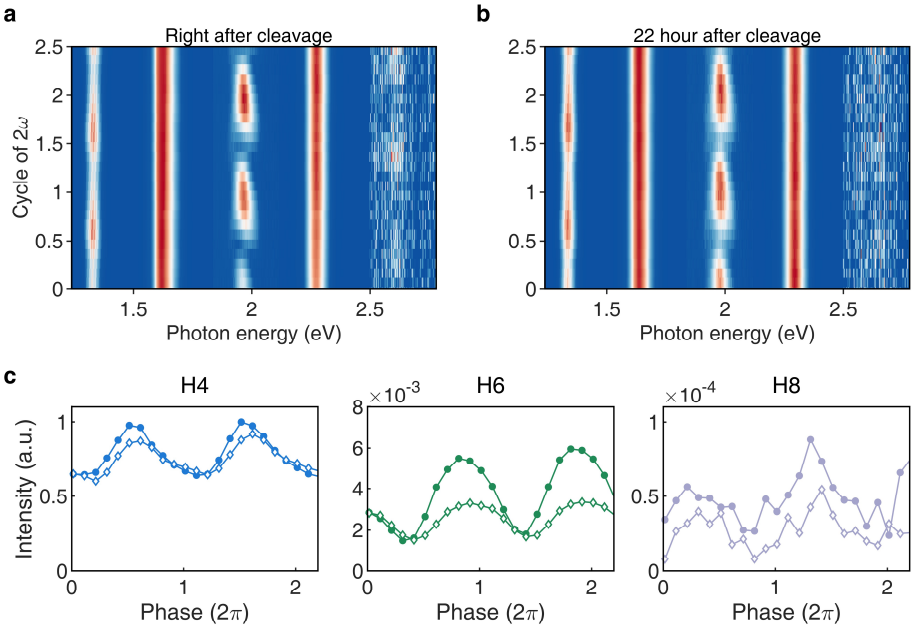

Fig. S1. a,b High-harmonic modulation from BSTS right after cleaving the crystal in air (**a**), and exposing the cleaved surface in ambient conditions for 22 hours (**b**). **c**. Comparison of the intensity oscillation of even-order harmonics (H4, H6, H8). Harmonic yields extracted from (**a**) are plotted in solid points, whereas that from (**b**) are drawn in white diamonds.

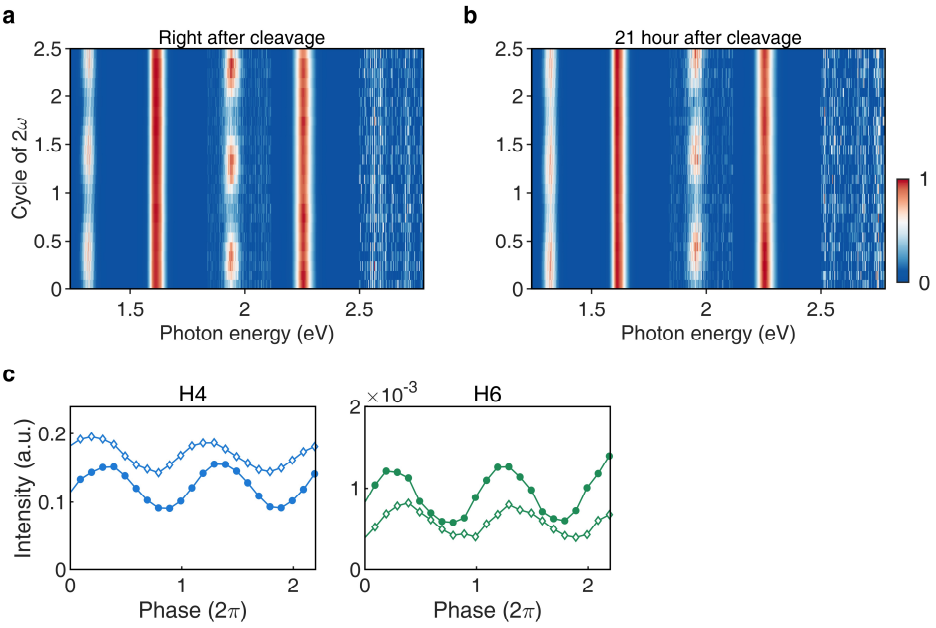

Fig. S2. a,b High-harmonic modulation from BIS right after cleaving the crystal in air (**a**), and exposing the cleaved surface in ambient conditions for about 21 hours (**b**). **c**. Comparison of the intensity oscillation of even-order harmonics (H4, H6). Harmonic yields extracted from (**a**) are plotted in solid points, whereas that from (**b**) are drawn in white diamonds. The intensity of H8 is not shown, as the signal of which is buried in background noises.

3. Tight binding Hamiltonian

The electronic structure of topological surface states can be obtained through the tight-binding model[S7], resulting in an effective Hamiltonian written as

$$\boldsymbol{H}(\boldsymbol{k}) = [h_0(\boldsymbol{k}) + \frac{B_0(h_5^{\Gamma} - h_5(\boldsymbol{k}))}{B_{11}}]\mathbf{I}_2 + \sqrt{1 - \frac{B_0^2}{B_{11}^2}}[h_1(\boldsymbol{k})\boldsymbol{\sigma}_x + h_2(\boldsymbol{k})\boldsymbol{\sigma}_y + h_3(\boldsymbol{k})\boldsymbol{\sigma}_z], \quad (1)$$

where $\boldsymbol{I}_2$ is the 2x2 identity matrix, $\boldsymbol{\sigma}_{x,y,z}$ are Pauli matrices, and other quantities are explicitly defined as

$$h_0(\boldsymbol{k}) = 2A_0 \sum_{i=1}^{3} \cos(\boldsymbol{k} \cdot \mathbf{a}_\mathrm{i}) + 2B_0 \sum_{i=1}^{3} \cos(\boldsymbol{k} \cdot \mathbf{a}_\mathrm{i}), \quad (2)$$

$$h_1(\boldsymbol{k}) = 2A_{14} \sin\frac{2\pi}{3}[\sin(\boldsymbol{k} \cdot \mathbf{a}_2) - \sin(\boldsymbol{k} \cdot \mathbf{a}_3)]$$

$$+2B_{14}[\sin(\boldsymbol{k} \cdot \mathbf{b}_1) + \sin\frac{2\pi}{3}(\sin(\boldsymbol{k} \cdot \mathbf{b}_2) + \sin(\boldsymbol{k} \cdot \mathbf{b}_3))] \quad (3)$$

$$h_2(\boldsymbol{k}) = 2B_{14} \sin\frac{2\pi}{3}[\sin(\boldsymbol{k} \cdot \mathbf{b}_2) - \sin(\boldsymbol{k} \cdot \mathbf{b}_3)]$$

$$-2A_{14}[\sin(\boldsymbol{k} \cdot \mathbf{a}_1) + \cos\frac{2\pi}{3}(\sin(\boldsymbol{k} \cdot \mathbf{a}_2) + \sin(\boldsymbol{k} \cdot \mathbf{a}_3))] \quad (4)$$

$$h_3(\boldsymbol{k}) = 2A_{12} \sum_{i=1}^{3} \sin(\boldsymbol{k} \cdot \mathbf{a}_\mathrm{i}) \quad (5)$$

$$h_4(\boldsymbol{k}) = -2B_{12} \sum_{i=1}^{3} \sin(\boldsymbol{k} \cdot \mathbf{b}_\mathrm{i}), \quad (6)$$

$$h_5(\boldsymbol{k}) = 2A_{11} \sum_{i=1}^{3} \cos(\boldsymbol{k} \cdot \mathbf{a}_\mathrm{i}) + 2B_{11} \sum_{i=1}^{3} \cos(\boldsymbol{k} \cdot \mathbf{b}_\mathrm{i}) + \mathfrak{m}_{11}. \quad (7)$$

where $\mathbf{a}_\mathrm{i}$ and $\mathbf{b}_\mathrm{i}$ (i=1,2,3) are the nearest-neighbor vectors (Extended Data Fig. 4a), and tight-binding parameters (in units of eV) for surface mode are chosen as $A_0 = -0.0255$, $A_{11} = 0.1937$, $A_{12} = 0.2240$, $A_{14} = 0.0551$, $B_0 = 0.0164$, $B_{11} = 0.1203$, $B_{12} = 0.3263$, $B_{14} = 0$, and $\mathfrak{m}_{11} = -1.6978$.

4. Semiclassical Bloch equation

The ultrafast electron dynamics of surface states irradiated by the intense two-colour laser fields can be described by two-band semiconductor Bloch equations (SBEs)[S8-S11]. We formulate the SBE within a frame of crystal momentum $\boldsymbol{k} = \boldsymbol{k}_0 + \boldsymbol{A}(t)$ moving with the vector potential $\boldsymbol{A}(t) = -\int_{-\infty}^{t} \boldsymbol{F}(\tau)\, d\,\tau$, where $\boldsymbol{F}(\tau)$ is the time-dependent electric field of laser pulses. Hence, the resulting SBE at a fixed initial $\boldsymbol{k}_0$ reads

$$\frac{d}{dt} P_{\boldsymbol{k}_0}(t) = -i[\mathcal{E}_g(\boldsymbol{k}) - \boldsymbol{F}(t)\cdot \Delta\boldsymbol{\mathcal{A}}(\boldsymbol{k})]P_{\boldsymbol{k}_0}(t) - i\boldsymbol{F}(t)\cdot \boldsymbol{d}_{\mathrm{cv}}(\boldsymbol{k}) w_{\boldsymbol{k}_0}(t) - \frac{P_{\boldsymbol{k}_0}(t)}{T_2} \quad (8)$$

and

$$\frac{d}{dt} f_{\mathrm{m}}^{\boldsymbol{k}_0}(t) = i2\,\mathrm{sgn}_{\mathrm{m}}\, \Im\mathfrak{m}[\,\boldsymbol{F}(t)\cdot \boldsymbol{d}_{\mathrm{cv}}(\boldsymbol{k}) P^{*}_{\boldsymbol{k}_0}(t)], \quad (9)$$

where $f_{\mathrm{m}}^{\boldsymbol{k}_0}$ represent the valence ($\mathrm{m} = \mathrm{v}$) and conduction ($\mathrm{n} = \mathrm{c}$) band population, $P_{\boldsymbol{k}_0}$ is the interband polarization, $w_{\boldsymbol{k}_0}(t) = f_{\mathrm{v}}^{\boldsymbol{k}_0}(t) - f_{\mathrm{c}}^{\boldsymbol{k}_0}(t)$ is the population difference, and $\Im\mathfrak{m}$ function returns the imaginary part of the complex variable. Here, the $\mathcal{E}_{\mathrm{g}}(\boldsymbol{k}) = \mathcal{E}_{\mathrm{c}}(\boldsymbol{k}) - \mathcal{E}_{\mathrm{v}}(\boldsymbol{k})$ is the energy different between the conduction and the valence bands. The $\Delta\boldsymbol{\mathcal{A}}(\boldsymbol{k}) = \boldsymbol{d}_{\mathrm{cc}}(\boldsymbol{k}) - \boldsymbol{d}_{\mathrm{vv}}(\boldsymbol{k})$ denotes the combined Berry connection between the two bands, which is sensitive to the crystal symmetry, with $\Delta\boldsymbol{\mathcal{A}}(\boldsymbol{k}) = 0$ for bulk bands and $\Delta\boldsymbol{\mathcal{A}}(\boldsymbol{k}) \neq 0$ for surface states. The $\mathrm{sgn}_{\mathrm{m}} = 1$ is for valence band and $\mathrm{sgn}_{\mathrm{m}} = -1$ is for conduction band.

We mainly consider the interband current due to its predominant contribution to even harmonic spectrum (Fig. S3). In order to gain a deeper physical insight, it is useful to write the interband current using Keldysh approximation $w_{\boldsymbol{k}_0}(t) \approx 1$ in an analytical form of

$$J_{\mathrm{er}}^{\mu}(t) = -\int_{\mathrm{BZ}} d^2\boldsymbol{k}\, \mathcal{E}_{\mathrm{g}}(\boldsymbol{k}) |d_{\mathrm{cv}}^{\mu}(\boldsymbol{k})| \int_{-\infty}^{t} |\boldsymbol{F}(t')\cdot \boldsymbol{d}_{\mathrm{cv}}(\kappa(t,t'))\,| e^{-iS_{\mu}(t',t,\boldsymbol{k}) - \frac{t-t'}{T_2}} dt' + \mathrm{c.c.} \quad (10)$$

where the accumulated phase is

$$S_{\mu}(t',t,\boldsymbol{k}) = \int_{t'}^{t} (\mathcal{E}_{\mathrm{g}}^{\boldsymbol{\kappa}(t,\tau)} - \boldsymbol{F}(\tau)\cdot \Delta\boldsymbol{\mathcal{A}}^{\boldsymbol{\kappa}(t,\tau)}) d\tau + \alpha_{\mu}^{\boldsymbol{k}} - \beta^{\boldsymbol{\kappa}(t,t')} \quad (11)$$

with $\mu = \{x, y\}$ the Cartesian indices, $\boldsymbol{\kappa}(t,t') = \boldsymbol{k} - \boldsymbol{A}(t) + \boldsymbol{A}(t')$, the transition dipole phase $\alpha_{\mu}^{\boldsymbol{k}} = \arg[\,\boldsymbol{d}_{\mathrm{cv}}^{\mu}(\boldsymbol{k})]$, and $\beta^{\kappa(t,t')} = \arg[\,\boldsymbol{F}(t')\cdot \boldsymbol{d}_{\mathrm{cv}}(\kappa(t,t'))]$.

The SBEs are numerically solved for each independent k-point by the classical fourth-order Runge-Kutta method. We sample 400 × 400 k-points with uniform grid spacing along two nonorthogonal primitive reciprocal vectors. For the bulk states, the band structure is three-dimensional. To mitigate excessive computational requirements, we adopted a procedure outlined in Ref. S7, where we solved the SBEs specifically within the (k_x, k_y, k_z=0) time-reversal-invariant plane.

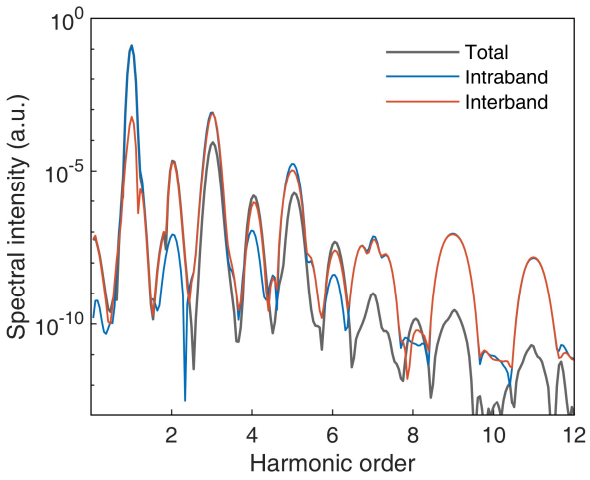

Fig. S3 The computed HHG from surface states driven by fundamental field only. The harmonic spectrum (gray line) is a composite of emissions from interband transition (red line) and intraband motion (blue line) of light field excited carriers.

References

S1. Luu, T. T. & Wörner, H. J. Observing broken inversion symmetry in solids using two-color high-order harmonic spectroscopy. *Phys. Rev. A* **98**, 041802 (2018).

S2. Vampa, G., Liu, H., Heinz, T. F. & Reis, D. A. Disentangling interface and bulk contributions to high-harmonic emission from solids. *Optica* **6**, 553-556 (2019).

S3. Bianchi, M. *et al.* Coexistence of the topological state and a two-dimensional electron gas on the surface of Bi_2Se_3. *Nat. Commun.* **1**, 128 (2010).

S4. Analytis, J. G. *et al.* Bulk Fermi surface coexistence with Dirac surface state in Bi_2Se_3: A comparison of photoemission and Shubnikov--de Haas measurements. *Phys. Rev. B* **81**, 205407 (2010).

S5. Benia, H. M., Lin, C., Kern, K. & Ast, C. R. Reactive chemical doping of the Bi_2Se_3 topological insulator. *Phys. Rev. Lett.* **107**, 177602 (2011).

S6. King, P. D. C. *et al.* Large tunable Rashba spin splitting of a two-dimensional electron gas in Bi_2Se_3. *Phys. Rev. Lett.* **107**, 096802 (2011).

S7. Baykusheva, D. *et al.* Strong-field physics in three-dimensional topological insulators. *Phys. Rev. A* **103**, 023101 (2021).

S8. Haug, H. & Koch, S. W. *Quantum theory of the optical and electronic properties of semiconductors* (World Scientific, Singapore, 2009).

S9. Li, J. *et al.* Phase invariance of the semiconductor Bloch equations. *Phys. Rev. A* **100**, 043404 (2019).

S10. Jiang, S. *et al.* Role of the transition dipole amplitude and phase on the generation of odd and even high-order harmonics in crystals. *Phys. Rev. Lett.* **120**, 253201 (2018).

S11. Yue, L. & Gaarde, M. B. Introduction to theory of high-harmonic generation in solids: tutorial. *J. Opt. Soc. Am. B* **39**, 535-555 (2022).